Synthesis and magnetic properties of Mn-doped $Cd_{0.1}Zn_{0.9}GeAs_2$ solid solutions

2008 J. Phys.: Condens. Matter 20 335220

(http://iopscience.iop.org/0953-8984/20/33/335220)

J. Phys.: Condens. Matter **20** (2008) 335220 (5pp) doi:10.1088/0953-8984/20/33/335220

Synthesis and magnetic properties of Mn-doped $Cd_{0.1}Zn_{0.9}GeAs_2$ solid solutions

A V Kochura[1,2], R Laiho[3], A Lashkul[1,3], E Lähderanta[1], M S Shakhov[1,4], I S Zakharov[2], S F Marenkin[5], A V Molchanov[5], S G Mikhailov[5] and G S Jurev[6]

[1] Department of Mathematics and Physics, Lappeenranta University of Technology, Lappeenranta, PO Box 20, FIN-53851, Finland
[2] Kursk State Technical University, ul. 50 let Oktyabrya 94, Kursk 305040, Russia
[3] Wihuri Physical Laboratory, University of Turku, Turku, FIN-20014, Finland
[4] A F Ioffe Physico-Technical Institute, 194021 St Petersburg, Russia
[5] Kurnakov Institute of General and Inorganic Chemistry, Russian Academy of Sciences, Leninskii prospect 31, Moscow 119991, Russia
[6] Institute of Inorganic Chemistry, Siberian Division, Russian Academy of Sciences, prospect Akademika Lavrent'eva 3, 630090 Novosibirsk, Russia

Received 30 April 2008, in final form 2 July 2008
Published 28 July 2008
Online at stacks.iop.org/JPhysCM/20/335220

Abstract
Homogeneous crystals of diluted magnetic semiconductor solid solution $Zn_{0.9}Cd_{0.1}GeAs_2$ doped with 0, 1.13 and 2.65 mass% of Mn were synthesized. The grown crystals were characterized by atomic absorption and synchrotron x-ray powder diffraction analyses showing that the lattice parameter of the sample crystals are closely related to GaAs. Measurements of magnetic and transport properties were performed in the temperature range of 4–400 K using steady and pulsed magnetic fields up to $B = 50$ and 150 kG, respectively. The ferromagnetic Curie temperature of the sample crystals was found to be about 350 K. The magnetic ordering is attributed to the presence of MnAs clusters with mean size ~3.8 nm in the ferromagnetic phase. Influence of paramagnetic Mn^{2+} ions on magnetic properties of the crystals was observed only at low temperatures and was explained by the p–d interaction between charge-carrying holes and localized Mn moments.

1. Introduction

The discovery of hole-mediated ferromagnetism (FM) in (III, Mn)V compounds [1] and progress in non-equilibrium growth of the diluted magnetic semiconductor GaAs:Mn [2] with Curie temperature up to $T_c = 173$ K [3] has encouraged research of other semiconductors structurally and chemically closely related to the III–V group. The valences in group III atoms and the double cation II–IV complexes are equal but the latter ones can contain more Mn than the III–V compounds, without forming a second phase. Observations of room-temperature ferromagnetism in II–IV–V_2 semiconductors doped with Mn [4–6], as well as theoretical calculations [7], have directed interest to new magnetic II–IV–V_2 materials. In this connection the Mn-doped room-temperature ferromagnetic (FM) chalcopyrite compounds $CdGeAs_2$ ($T_c = 355$ K) [6] and $ZnGeAs_2$ ($T_c = 333$ K) [5] have attracted attention because of their optical and structural properties [8, 9], which are interesting for applications. In the present work we investigate growth and magnetic properties of pure and Mn-doped $Cd_{0.1}Zn_{0.9}GeAs_2$ solid solutions.

2. Experimental procedure

High-purity (99.999%) Ge and Mn powders were used for synthesis of $Cd_{0.1}Zn_{0.9}GeAs_2$:Mn solid solutions from crystalline starting materials $CdAs_2$ and $ZnAs_2$ prepared by the vertical Bridgman technique. The starting materials were ground to powders with average particle size 5–10 μm and batches of 9–10 g weighed with an accuracy of 0.005% were loaded into quartz ampoules coated with pyrolytic graphite and evacuated to 1×10^{-2} Pa. The synthesis temperature and duration were 902 °C and 36 h, respectively. To maximize the solubility of Mn in the host lattice the cooling rate of the melt was adjusted to 10–12 K s^{-1}. Three samples with 0, 1.13 and 2.65 mass% of Mn were grown and labeled as #1, #2 and #3,

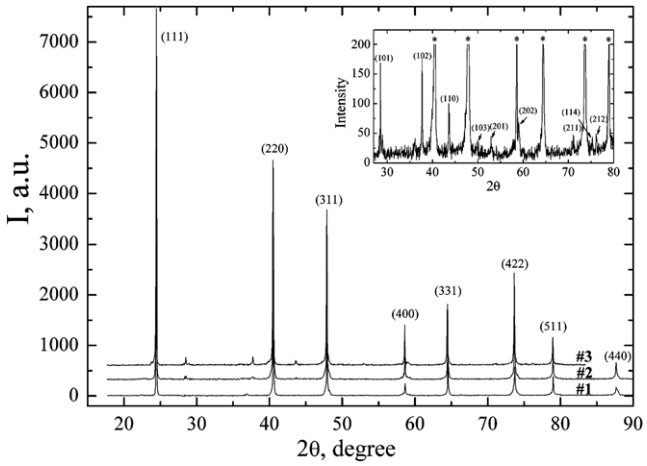

Figure 1. Synchrotron x-ray diffraction patterns of $Cd_{0.1}Zn_{0.9}GeAs_2$ with Mn. Inset: enlarged part of the diffraction pattern of sample #3 with Miller indexes shown for MnAs ($P6_3/mmc$: $a = 4.139$ Å, $c = 5.753$ Å) and diffraction peaks of $Cd_{0.1}Zn_{0.9}GeAs_2$ labeled by stars.

respectively. The composition of the crystals was studied with atomic absorption analysis in the center and at the periphery of the ingots. For detection of possible II-As_2 and II_3-As_2 minority phases synchrotron x-ray powder diffraction analysis was carried out at diffracted wavelength $\lambda = 1.3828(1)$ Å with $\Delta 2\theta = 0.01°$ steps of high-angle (400) reflections from an Si single crystal.

Magnetization of the samples was measured between 5–310 K and 260–400 K in fields up to $B = 50$ kG using a superconducting quantum interference device (SQUID) magnetometer. Before every measurement the sample was annealed for 0.5–1 h at 420 K to remove possible remanent magnetization. The electrical and magnetotransport properties were investigated between 4.2 and 320 K using the standard six-point geometry in pulsed magnetic fields up to 180 kG. The samples had high conductivity and linear current–voltage characteristics in the range of the measurements.

3. Results

The x-ray diffraction patterns analyzed with the help of the ICSD database (2005) are shown in figure 1. It was found that instead of the usual II–IV–V_2 tetragonal chalcopyrite $I4/2d$ structure the $Cd_{0.1}Zn_{0.9}GeAs_2$:Mn samples were crystallized according to metastable cubic-like zinc blende structure $F4/3m$ with lattice parameter $a = 5.644$ Å [10]. As expected, the lattice parameter of sample #1 ($a = 5.648(1)$ Å) exceeded that of cubic $ZnGeAs_2$ (figure 2(b)) due to partial replacement of Zn by Cd. The lattice parameter of sample #2 was not changed, but that of sample #3 was increased up to 5.651(1) Å, practically coinciding with the lattice constant of GaAs (5.653 Å). With increasing Mn content the intensities of the MnAs diffraction peaks (hexagonal NiAs-type phase, $P6_3/mmc$) increased almost in proportion to the amount of Mn in the samples. In zero magnetic field at $T < 306$ K and $T > 394$ K the MnAs has hexagonal structure and at 306 K $< T <$ 394 K the MnP-type orthorhombic structure ($Pnma$) [11]. When analyzing the magnetic properties of the samples it is necessary to take into account, that the Curie temperature of the transitions from the hexagonal FM to orthorhombic paramagnetic (PM) phase [11] depends not only on the value of the applied magnetic field B, but on the measurement mode: in zero field $T_{Cc} = 306$ K on cooling and $T_{Ch} = 317$ K on heating. When B is increased from 0 to 60 kG the values of T_{Ch} and T_{Cc} are shifted to higher temperatures by about 20 and 30 K, respectively. In the PM orthorhombic phase the magnetic moment per Mn atom is about 2 μ_B compared to 3.4 μ_B in the hexagonal FM phase [11].

The measurements made between 4.2 and 400 K at $B = 50$ kG show that the pure material (sample #1) is diamagnetic with $|\chi| = 4 \times 10^{-7}$ emu g^{-1} G^{-1}. When analyzing the magnetic properties of the Mn-containing samples this diamagnetic contribution was subtracted from the data. The coercive force at 5 K was 25 and 40 G for samples #2 and #3, respectively (figure 3).

The temperature dependences of the magnetization $M(T)$ measured after cooling the sample in zero field (ZFC) ($B <$ 0.1 G) and while cooling in a field (FC) are shown in figure 4.

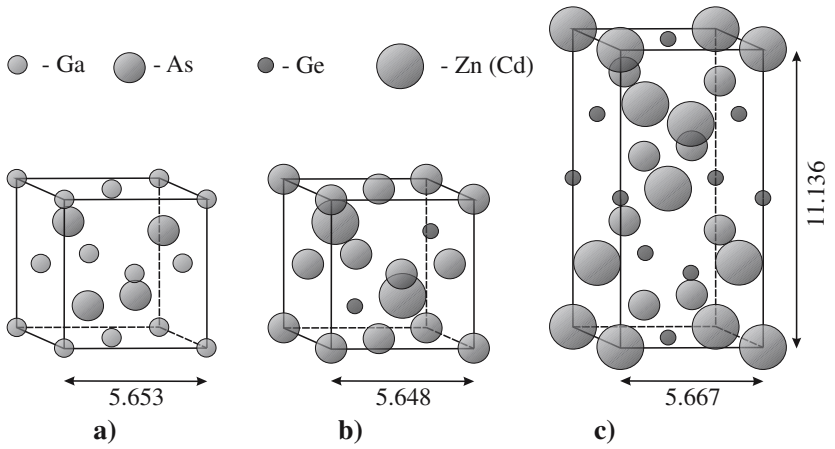

Figure 2. Unit cells: (a) GaAs; (b) $Cd_{0.1}Zn_{0.9}GeAs_2$ and (c) chalcopyrite $ZnGeAs_2$. Crystal lattice parameters are in ångström units.

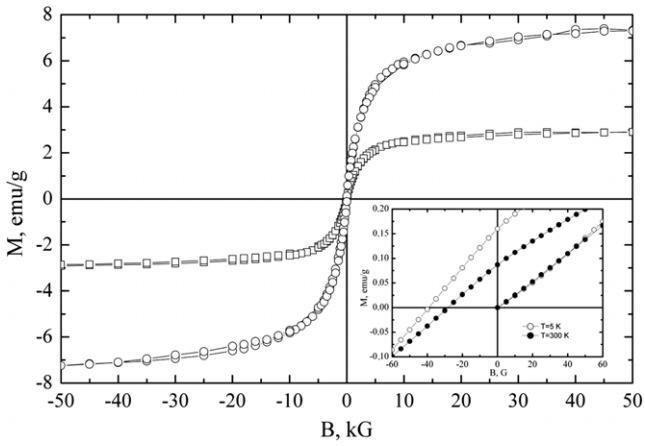

Figure 3. Magnetization $M(B)$ for samples #2 (open squares) and #3 (open circles) measured at $T = 5$ K. Inset: part of the low field hysteresis loop for sample #3.

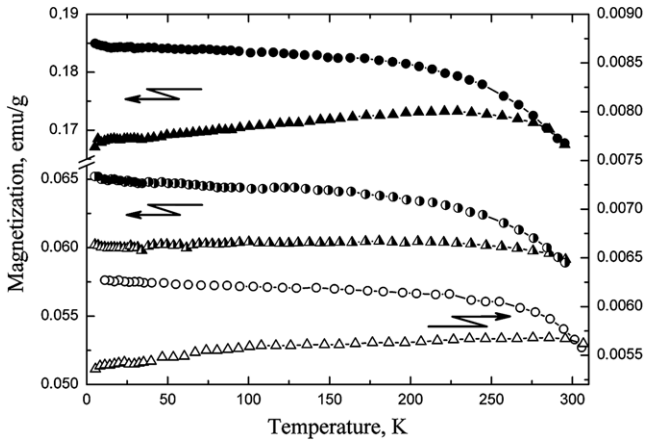

Figure 4. Temperature dependence of M_{ZFC} (triangles) and M_{FC} (circles) for sample #2 (open symbols), sample #3 (half-filled symbols) at $B = 5$ G and sample #3 (solid symbols) at $B = 50$ G.

The difference between the FC and ZFC curves decreased with increasing the field and disappeared at $B > 10$ kG. The broad maximum of the $M_{ZFC}(T)$ curve around $T_b \approx 250$ K is more pronounced in sample #3.

As shown in figure 5 a rapid increase of the magnetization is observed below 25 K in the $M(T)$ curve measured at 50 kG. Upon increasing the temperature the decrease of the magnetization becomes slower, but starts to decrease rapidly again above $T \approx 300$ K, indicating the presence of a magnetic transition. For sample #2 the value of $T_c = 349$ K at 50 kG was obtained from extrapolation of the steepest part of the $M(T)$ curve until it intersects the T axis. No remanent magnetization around this temperature was observed. The data of $M(T)$ in low (500 G) and zero fields gave the values of $T_c = 327$ and 323 K, respectively. An extrapolation of the linear high-temperature part of the inverse susceptibility at $B = 50$ kG gives the PM Curie temperature 324 ± 6 K for sample #2 (figure 5, inset). For sample #3 with higher Mn content the values of the critical temperatures differ from those given above by no more than 3 K, which is within the limits of errors.

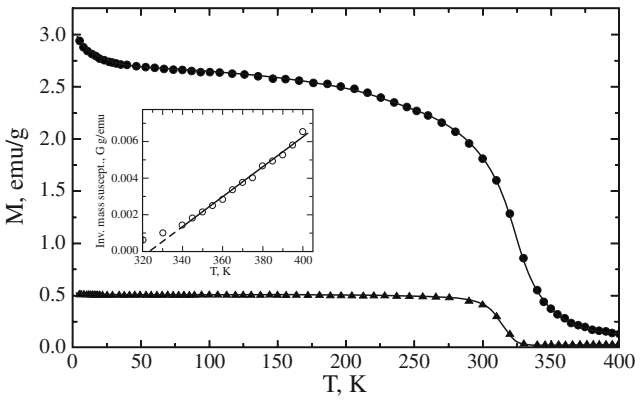

Figure 5. Temperature dependence of the magnetization for sample #2 measured at $B = 500$ G (triangles) and $B = 50$ kG (circles). Inset: temperature dependence of the inverse susceptibility above T_C.

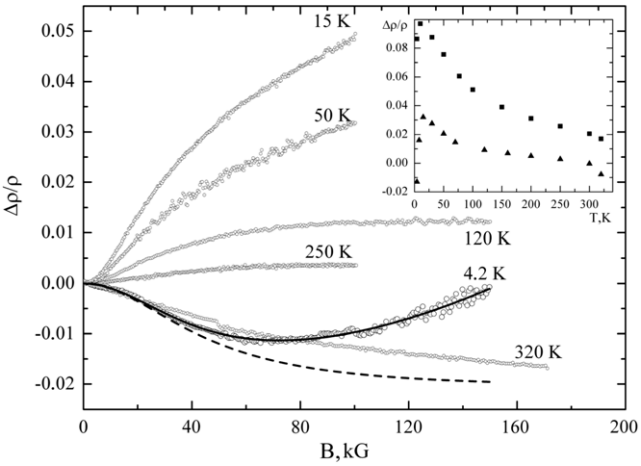

Figure 6. Magnetic field dependence of the magnetoresistance for sample #3 at different temperatures. The continuous line corresponds to the best fitting parameters at $T = 4.2$ K. The dashed line represents the Brillouin term (equation (3)). Inset: the temperature dependence of the magnetoresistance $\Delta\rho/\rho$ for samples #2 (squares) and #3 (triangles) at $B = 50$ kG.

The pure sample #1 had a low positive magnetoresistance $\Delta\rho/\rho = (\rho_B - \rho_0)/\rho_0$ of 1.1% at $B = 50$ kG and $T = 300$ K. The temperature dependences of $\Delta\rho/\rho$ of samples #2 and #3 at $B = 50$ kG are shown in figure 6. Sample #3 at $T = 4.2$ K had magnetoresistance up to -1.2%, consisting of a negative component prevailing up to 60 kG, and an upturn between 60 and 150 kG, due to a positive contribution.

Thermal emf measurements showed that the samples had p-type conductivity with charge carrier concentration $p_2 = 1.4 \times 10^{20}$ and $p_3 = 1.0 \times 10^{20}$ cm^{-3} at $T = 4.2$ K for #2 and #3, respectively. With increasing temperature these values slowly increased to $p_2 = 1.9 \times 10^{20}$ and $p_3 = 1.3 \times 10^{20}$ cm^{-3} observed at 300 K.

4. Discussion

The synchrotron radiation patterns together with deviation of the ZFC and FC magnetization curves below $T = 290$ K

and the maximum in the ZFC curves at $T_b \approx 250$ K give strong evidence that the magnetic properties of our $Cd_{0.1}Zn_{0.9}GeAs_2$:Mn samples are governed by the presence of MnAs clusters, as observed in the II–V [12–14] and III–V [15–17] diluted magnetic semiconductors. From the difference between the saturation magnetization of MnAs, $\sigma_s \approx 123$ emu g^{-1} (260 K) [18], and the magnetization of our samples at $T = 260$ K and $B = 50$ kG, it was estimated that the mass fraction of MnAs was $\eta = 0.0186$ and 0.0479, and that of Mn was $\beta = 0.0036$ and 0.0063 in samples #2 and #3, respectively. The small difference between the lattice parameters of these samples also indicates that β has to be small. Changing of the lattice parameter in $Cd_{0.1}Zn_{0.9}GeAs_2$ by doping with Mn is most probably due to substitution of Mn^{2+} for Cd or Zn in the form of isoelectronic centers. On these positions the Mn atom contributes electrons to bonding with As neighbors. In fourfold coordination the effective radius of Mn^{2+} is 0.66 Å and the radii of Zn^{2+} and Cd^{2+} are 0.6 and 0.78 Å, respectively, while the radius of Ge^{4+} is 0.39 Å [19]. As the lattice parameters of the undoped sample #1 and sample #2 with 1.13% were similar, it is likely that Mn at small concentrations replaces mostly Zn^{2+} or Cd^{2+}, as in $CdGeAs_2$:Mn [20, 21] where Mn^{2+} ions can substitute Ge^{4+}, supplying holes to the valence band. It is worth noting that Cr^{2+} ions in $CdGeAs_2$ go preferentially to the Cd site in heavily doped crystals but that the growth conditions and stoichiometry may play a role in Cr incorporation on each cation site [22].

In the field of $B = 50$ kG the contribution of the MnAs clusters to net magnetization $M_{FM}(T) = \eta\rho\sigma_s(T)$, where $\rho = 4.84$ g cm^{-3} is the mass density of the sample, is practically saturated while the paramagnetic magnetization of free Mn ions $M_{PM}(T) \approx \chi_{PM}(T)B$ is still sufficiently far from saturation. Here $\chi_{PM} = C/(T - \theta_{CW})$, where $C = p_{eff}^2 \mu_B N/3k_B$ is the Curie constant, p_{eff} is the effective number of Bohr magnetons μ_B per Mn ion, N is the concentration of Mn outside the MnAs clusters and θ_{CW} is the Curie–Weiss temperature. We found the saturation of magnetization $\sigma_s(T)$ with the help of interpolation by a rational beta-spline function taking basic data from [18] and extrapolating by a linear function at low temperatures. From the best fit of $M(T)$ we obtain the values of $p_{eff}^2 \approx 20$ and 25 for samples #2 and #3, respectively, which are smaller than the effective Bohr magneton number for free Mn^{2+} ($p_{eff}^2 \approx 35$).

Similar to $Zn_{1-x}Mn_xAs_2$ [13] and $(Zn_{1-x}Mn_x)_3As_2$ [14] the blocking temperature of FM MnAs particles is [23]

$$T_b = \frac{KV}{25k_B} \tag{1}$$

where K is the density of the anisotropy energy and V is the average volume of the particles. The distribution function of T_b can be calculated from [13]

$$f(T_b) = \frac{1}{\gamma}\frac{d}{dT}\left[\frac{T\chi_{ZFC}(T)}{\sigma_s^2(T)}\right] - \lambda. \tag{2}$$

The distribution function $f(R)$ of the radius of the sphere corresponding to the cluster volume is calculated using equation (1) and the temperature dependences of K and σ_s [18]. The constants λ and γ are determined by normalizing $f(R)$ to unity and using the condition $f(R) = 0$ at $R = 0$ (figure 7). Fitting $f(R)$ with a Gaussian function gives the most probable radius of the clusters $R_2 = 3.7$ nm with mean-square deviation $\delta_2 = 1.0$ nm for sample #2 and $R_3 = 3.8$ nm and $\delta_3 = 1.1$ nm for sample #3.

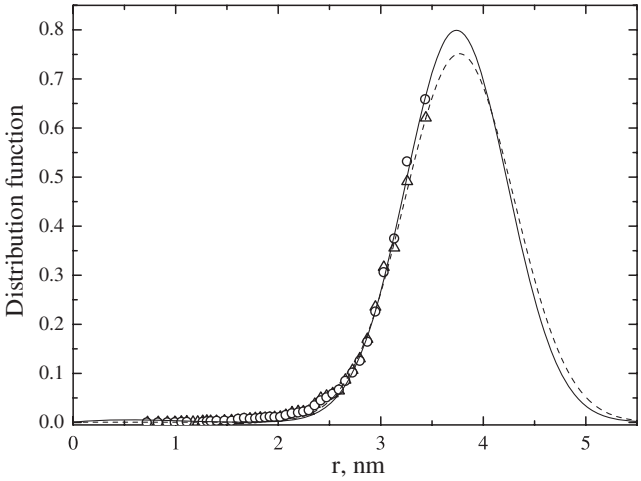

Figure 7. The distribution functions of the cluster radius calculated with Gaussian function for samples #2 (circles, dashed line) and #3 (triangles, continuous line). The distributions parameters are given in the text. Experimental data points are calculated using equations (1) and (2).

In the range of temperatures from 15 to 250 K the magnetoresistance $\Delta\rho/\rho$ can be described by a classical model for positive magnetoresistance when two types of noninteracting carriers are present [24]. Furthermore, the shapes of the temperature dependences of the ratio $\Delta\rho/\rho$ (figure 6, inset) above 15 K are close to those in epitaxially grown MnAs with two types of carriers [25]. At $T > 300$ K the influence of the MnAs minority phase of samples #2 and #3 is revealed as a bend of $\Delta\rho/\rho$ towards negative values (figure 6, inset), which accompanies the transition from a FM NiAs-type hexagonal to a PM orthorhombic phase [25, 26].

Significant influence of the Mn ions on $\Delta\rho/\rho$ at low temperatures was observed only for sample #3. Magnetoresistance at 4.2 K consists of a positive quadratic term $(\Delta\rho/\rho)_p$ (ordinary magnetoresistance) and a negative term $(\Delta\rho/\rho)_n$, which depends on the Brillouin function. Such behavior can be explained assuming p–d exchange interaction between spin-polarized charge carriers and Mn^{2+} ions ($S = 5/2$) localized outside the magnetically ordered regions [27]. Above T_c the negative term can be expressed by the equation [27]

$$\left(\frac{\Delta\rho}{\rho}\right)_n = -\frac{J_{pd}^2}{V_{int}^2}\left[4\langle S_Z\rangle^2 + \langle S_Z\rangle\left(\coth\frac{\alpha}{2} - \frac{\alpha}{2\sinh^2\frac{\alpha}{2}}\right)\right], \tag{3}$$

where J_{pd} is the coupling constant, V_{int} is the spin-independent part of the Hamiltonian for interaction between delocalized holes and for the 3d shells of the Mn^{2+} ions, $\langle S_Z\rangle$ is given by the Brillouin function $B_{5/2}(\alpha)$ with argument

$\alpha = (g\ \mu_B B)/k_B T_{eff}$ and the effective temperature $T_{eff} = T - T^*$, where a simple mean field theory predicts T^* very close to T_C. After separation of the magnetoresistance to the Brillouin term (figure 6, dashed line) and the quadratic terms $(\Delta\rho/\rho)_p$ we find $J_{pd}/V = 0.064$ and $T^* = 1.5$ K by fitting $(\Delta\rho/\rho)_n$ to equation (3). This points out the possibility of low-temperature FM ordering due to coupled Mn^{2+} moments in $Cd_{0.1}Zn_{0.9}GeAs_2$ doped with Mn up to 2.65 mass%.

5. Conclusions

$Cd_{0.1}Zn_{0.9}GeAs_2$:Mn solid solutions having ferromagnetic properties with $T_c \approx 350$ K and lattice parameters differing from that of GaAs less than 0.04% are synthesized. The high-temperature magnetic properties of the compound are determined by the presence of MnAs ferromagnetic nanoclusters of mean size 3.8 nm.

Influence of paramagnetic Mn^{2+} ions on magnetic properties caused by replacing II and IV atoms in the host lattice with Mn is observed at low temperatures. For the sample with Mn content 2.65 mass% magnetic ordering observed with fitting at temperatures less than 1.5 K can be described by p–d interaction between charge-carrying holes and localized Mn moments.

Acknowledgments

This work was supported by the International Association for Promotion of Co-operation with Scientists from the New Independent States of the former Soviet Union (INTAS) under grant no. 06-1000014-5792, the Centre for International Mobility (CIMO) under grant no. TM-06-4408 and by the Russian Fund of Basic Research (RFBR) under grant no. 07-03-00810.

References

[1] Ohno H, Munekata H, Penney T, von Molnár S and Chang L L 1992 *Phys. Rev. Lett.* **68** 2664
[2] Ohno H 1998 *Science* **281** 951
[3] Wang K Y, Campion R P, Edmonds K W, Sawicki M, Dietl T, Foxon C T and Gallagher B L 2005 *ICPS-27: Physics of Semiconductors: 27th Int. Conf. on the Physics of Semiconductors*; *AIP Conf. Proc.* **772** 333
[4] Sato K, Medvedkin G A, Ishibashi T, Mitani S, Takanashi K, Ishida Y, Sarma D D, Okabayashi J, Fujimori A, Kamatani T and Akai H 2003 *J. Phys. Chem. Solids* **64** 1461
[5] Choi S, Choi J, Hong S C, Cho S, Kim Y and Ketterson J B 2003 *J. Korean Phys. Soc.* **42** S739
[6] Demin R, Koroleva L, Marenkin S, Mikhailov S, Aminov T, Szymczak H, Szymczak R and Baran M 2005 *J. Magn. Magn. Mater.* **290/291** 1379
[7] Erwin S C and Zitic I 2004 *Nat. Mater.* **3** 410
[8] Solomon G S, Timmons M L and Posthill J B 1989 *J. Appl. Phys.* **65** 1952
[9] Boyd G D, Buehler E, Storz F G and Wernick J H 1972 *IEEE J. Quantum Electron.* **8** 419
[10] Vaipolin A A, Osmanov E O and Prochukhan V D 1972 *Izv. Akad. Nauk SSSR, Neorg. Mater.* **8** 825
[11] Pytlik L and Zieba A 1985 *J. Magn. Magn. Mater.* **51** 199
[12] Cisowski J 1997 *Phys. Status Solidi* b **200** 311
[13] Laiho R, Lisunov K G, Lahderanta E and Zakhvalinskii V S 1999 *J. Phys.: Condens. Matter* **11** 555
[14] Laiho R, Lisunov K G, Lahderanta E and Zakhvalinskii V S 1999 *J. Phys.: Condens. Matter* **11** 8697
[15] Ohno H, Munekata H, von Molnár S and Chang L L 1991 *J. Appl. Phys.* **69** 6103
[16] Moreno M, Trampert A, Jenichen B, Daweritz L and Ploog K H 2002 *J. Appl. Phys.* **92** 4672
[17] Wang K Y, Sawicki M, Edmonds K W, Champion R P, Rushforth A W, Freeman A A, Foxon C T, Gallagher B L and Dietl T 2006 *Appl. Phys. Lett.* **88** 022510
[18] De Blois R W and Rodbell D S 1963 *J. Appl. Phys.* **34** 1101
[19] Dean J A 1999 *Lange's Handbook of Chemistry* 15th edn (New York: McGraw-Hill) pp 4.30–4
[20] Novotortsev V M, Kalinnikov V T, Koroleva L I, Demin R V, Marenkin S F, Aminov T G, Shabunina G G, Boichuk S V and Ivanov V A 2005 *Russ. J. Inorg. Chem.* **50** 492
[21] Novotortsev V M, Palkina K K, Mikhailov S G, Molchanov A V, Ochertyanova L I and Marenkin S F 2005 *Inorg. Mater.* **41** 439
[22] Garces N Y, Giles N C, Halliburtion L E, Nagashio K, Feigelson R S and Schunemann P G 2003 *J. Appl. Phys.* **94** 7567
[23] Bean C P and Livingston J D 1959 *J. Appl. Phys.* **30** S120
[24] Ziman J M 1960 *Electrons and Phonons* (Oxford: Oxford University Press)
[25] Berry J J, Potashnik S J, Chun S H, Ku K C, Schiffer P and Samarth N 2001 *Phys. Rev.* B **64** 052408
[26] Mira J, Rivadulla F, Rivas J, Fondado A, Caciuffo R, Carsughi F, Guidi T and Goodenough J B 2003 *Phys. Rev. Lett.* **90** 189901
[27] Csontos M, Wojtowicz T, Liu X, Dobrovolska M, Janko B, Furduna J K and Mihaly G 2005 *Phys. Rev. Lett.* **95** 227203